Theoretical investigation of the He–I2(E3Πg) ion-pair state: Ab initio intermolecular potential and vibrational levels

Apostolos Kalemos, Álvaro Valdés, and Rita Prosmiti

Citation: J. Chem. Phys. **137**, 034303 (2012); doi: 10.1063/1.4733983
View online: http://dx.doi.org/10.1063/1.4733983
View Table of Contents: http://jcp.aip.org/resource/1/JCPSA6/v137/i3
Published by the American Institute of Physics.

Theoretical investigation of the He–$I_2(E^3\Pi_g)$ ion-pair state: *Ab initio* intermolecular potential and vibrational levels

Apostolos Kalemos,[1,a)] Álvaro Valdés,[2] and Rita Prosmiti[2,b)]
[1]*National and Kapodistrian University of Athens, Department of Chemistry, Laboratory of Physical Chemistry, Panepistimiopolis, Athens 15771, Greece*
[2]*Instituto de Física Fundamental, IFF-CSIC, Serrano 123, 28006 Madrid, Spain*

(Received 30 March 2012; accepted 21 June 2012; published online 17 July 2012)

We present a theoretical study on the potential energy surface and vibrational bound states of the E electronic excited state of the HeI_2 van der Waals system. The interaction energies are computed using accurate *ab initio* methods and large basis sets. Relativistic small-core effective core potentials in conjunction with a quintuple-zeta quality basis set are employed for the heavy iodine atoms in multireference configuration interaction calculations for the $^3A'$ and $^3A''$ states. For the representation of the potential energy surface we used a general interpolation technique for constructing potential surfaces from *ab initio* data based on the reproducing kernel Hilbert space method. The surface presents global and local minima for T-shaped configurations with well-depths of 33.2 and 4.6 cm^{-1}, respectively. Vibrational energies and states are computed through variational quantum mechanical calculations. We found that the binding energy of the $HeI_2(E)$ T-shaped isomer is 16.85 cm^{-1}, in excellent agreement with recent experimental measurements. In lieu of more experimental data we also report our predictions on higher vibrational levels and we analyze the influence of the underlying surface on them. This is the first attempt to represent the potential surface of such a highly excited electronic state of a van der Waals complex, and it demonstrates the capability of the *ab initio* technology to provide accurate results for carrying out reliable studies to model experimental data.
 [http://dx.doi.org/10.1063/1.4733983]

I. INTRODUCTION

Research on van der Waals (vdW) complexes has a long and rich history mainly due to their protagonist role in the study of energy transfer mechanisms and weak intermolecular forces.[1] Progress in both experimental techniques and computational methods during the last years has contributed to an improved understanding of these "simple" molecular entities (see Refs. 2–8 and references therein).

Rare gas (Rg) dihalogen systems (XY) represent an interesting class of vdW complexes with the He–I_2 system being the first to be studied experimentally by the Levy group through laser excited fluorescence spectroscopy as early as 1976.[9] At that time the He–$I_2(X^1\Sigma_g^+)$ system was predicted to have a C_{2v} (T-shaped) configuration characterized by a perpendicular distance $R_0 = 4.47 \pm 0.13$ Å (Ref. 10) and a binding energy, D_0, initially estimated at 18.8 ± 0.6 cm^{-1} (Ref. 11) but later revised to $D_0 = 17.6 \pm 1.0$ cm^{-1}.[12] The most recent experimental binding energy, reported by the Loomis group,[13] amounts to 16.6 ± 0.6 cm^{-1} for the C_{2v} conformer and 16.3 ± 0.6 cm^{-1} for the linear conformer. The double minimum topology of the potential energy surface (PES), an interesting feature *per* se, was a known experimental fact from the studies on Ar–I_2 (Refs. 14 and 15) and Ne–I_2 (Ref. 16) by the groups of Klemperer and Heaven. From a theoretical perspective, *ab initio* high level calculations have also predicted the existence of a double-minimum topology for such systems.[17–21] In the light of the latest experimental data by the Loomis group,[13] we recently revisited the He–$I_2(X)$ vdW complex.[22] Our estimates of 15.72 cm^{-1} (linear) and 15.51 cm^{-1} (T-shaped) for the binding energy are very close to each other and to the most recent experimental values.

In all these experimental studies[10–13] electronic excited states of the HeI_2 are involved, such as the $B(^3\Pi_{0_u^+})$ and $E(^3\Pi_{0_g^+})$ states, thus for any direct comparison between theoretical simulations and experimental measurements the knowledge of the underlying intermolecular interactions is mandatory. Information on these excited electronic states of such complexes based on *ab initio* computations is rather limited, and only recently calculations on the B state of some vdW systems, such as $HeCl_2$, $HeBr_2$, $NeCl_2$, and HeI_2, have been reported.[23–26]

Concerning the He–$I_2(B)$ system, we reported PES based on high level variational and coupled-cluster (CC) calculations that incorporate scalar relativity, while the spin–orbit (SO) coupling effects were considered indirectly by averaging the $^3A'$ and $^3A''$ surfaces.[26] A C_{2v} structure was found, bound by 12.33 cm^{-1} with a vibrationally averaged $R_0 = 4.58$ Å, in excellent agreement with the corresponding experimental findings of 12.8 ± 0.6 cm^{-1} and 4.79 ± 0.22 Å.[13]

Unfortunately, no theoretical results are available today for higher excited electronic states of either HeI_2 or any other similar Rg-XY vdW complex. As we mentioned above the E state of He–$I_2(E\ 0_g^+)$ vdW complex is involved in the experimental setup, although not experimentally studied until

a)E-mail: kalemos@chem.uoa.gr.
b)E-mail: rita@iff.csic.es.

recently (see Ref. 13). The Loomis's group, using two-laser, pump-probe spectroscopy, has accessed intermolecular vibrational levels associated with He–I_2(E 0_g^+, $v^\dagger = 0, 1$) ion-pair state.[13] The available experimental data are condensed in a T-shaped structure with the first vdW vibrational level lying at -16.7 ± 0.6 cm^{-1} that enabled them to set the binding energy for the corresponding PES of the system.

From a theoretical point of view, the E 0_g^+ state of the I_2 species, traditionally described as an ion–pair state,[27] was practically unexplored until very recently.[28] This state dissociates adiabatically to I($5s^2 5p^5$,^{2}P) + I*($5s^2 5p^4$(^{3}P)$6s^1$,^{4}P), a channel of mixed valence + Rydberg character. However, a severe avoided crossing at ∼25 Å with the ionic curve changes its character to an ion-pair one, i.e., I^-–I^+ ↔ I^+–I^- that is maintained up to ∼2.86 Å, where a second avoided crossing with an incoming $^3\Pi_g$ state confers a Rydberg character and creates a second (local) minimum. The existence of these two minima, a global featuring an ion-pair nature located at $r_e = 3.593$ Å and with a well-depth of 29799 cm^{-1}, and a local one of pure Rydberg character at $r_e = 2.589$ Å with a D_e of 21720 cm^{-1} with respect to the adiabatic I(^{2}P) + I*(^{4}P) dissociation limit, at the MRCI+Q level of theory,[28] is the most important characteristic of the I_2 E 0_g^+ potential curve. Consequently, a He atom can approach the I_2 E state at both its equilibrium minima resulting to an interesting polymorphic PES for the triatomic system. In this account, we study the interaction resulting when a He atom approaches I_2 only to its well established ion-pair minimum. To the best of our knowledge, this is the first *ab initio* report on the He–I_2(E) PES. Such potential surfaces are also of primary interest in studying the dynamics of non-adiabatic transitions in collisions of the I_2(E) with He atoms.[29,30] Due to the lack of *ab initio* PES, semiempirical models have been developed and employed in the quantum scattering calculations, although in these studies the importance of the correct description of the surface for the interpretation and modeling of the collision mechanisms is clearly indicated.[29–32]

In the present work, we use multireference configuration interaction (MRCI) methods, employing relativistic effective core potentials for the I atoms and large basis sets to compute the interaction energies and to provide an accurate description of the E ion-pair excited electronic state of the HeI_2 cluster. In Sec. II, we describe the methodological aspects of the *ab initio* computations, along with the procedure employed for the representation of the PES. As will be discussed below, the spin-orbit coupling effects can be accurately accounted for by averaging the $^3A'$ and $^3A''$ interaction potentials, and quantum vibrational bound-state calculations are carried out on this averaged surface. Our results on the MRCI interaction energies, binding energies, and structures, as well as their comparison to the available experimental data are presented and discussed in Sec. III. Final conclusions are given in Sec. IV.

II. COMPUTATIONAL DETAILS

A. *Ab initio* electronic structure calculations

The electronic configuration of the ground ^{2}P state of the I atom is [Ar]$3d^{10}4s^2 4p^6 4d^{10}5s^2 5p^5$. The [Ar+$3d^{10}$] electrons are described by the relativistic ECP28MDF effective core potential,[33] while for the $4s^2 4p^6 4d^{10}5s^2 5p^5$ electrons the aug-cc-pV5Z-PP basis set[33] is employed generally contracted to [8*s*8*p*6*d*4*f*3*g*2*h*]. The accuracy of small-core ECP and associated basis sets for the I_2 states correlating to the I(^{2}P) + I(^{2}P), I(^{2}P) + I*(^{4}P), I(^{2}P) + I*(^{2}P), and I^+(^{3}P) + I^-(^{1}S) asymptotes have been recently investigated.[26,28] For the He atom, the aug-cc-pVQZ basis set is used generally contracted to [5*s*4*p*3*d*2*f*].[34] Overall, the description of the triatomic system is achieved through 139×2 + 46 = 324 spherical Gaussian functions.

The approach of the He (^{1}S) atom to the I_2(E $^3\Pi_g$) state results in two PES of $^3A'$ and $^3A''$ symmetry, the Renner–Teller companions of the HeI_2($^3\Pi$) linear configuration. Jacobi coordinates (r, R, θ) are employed for the description of the PES of the HeI_2 complex, where R is the intermolecular distance of the He atom from the center of mass of I_2, r is the bond length of iodine, and θ is the angle defined by the **R** and **r** vectors. We constructed potential energy curves of both $^3A'$ and $^3A''$ symmetry for θ angles ranging from $\theta = 0^\circ$ ($C_{\infty v}$) to $\theta = 90^\circ$ (C_{2v}) with a step of 10°. At each θ value we calculated the interaction energy at R distances ranging from 3 to 30 Å. The r(I–I) interatomic distance has been kept frozen at its equilibrium $r_e = 3.5931$ Å value.[28] The total grid in $r \times R \times \theta$ (= $r_e \times$[3, 30 Å] × [0°, 90°]) consists in calculating the interaction energy of ∽ 1300 points in the configuration space.

Due to the multireference equilibrium character of the I_2 E state[28] we have employed a complete active space self-consistent field (CASSCF) zeroth order wavefunction that describes properly the triatomic system at every point of its configuration space. Dynamical correlation was extracted by single and double replacements out of the reference wavefunction (CASSCF+1+2 = MRCI), while the internally contraction scheme as implemented in the MOLPRO 2006 package[35] was used in order to keep the CI spaces at manageable levels. The He–I_2(E) $^3A'$ corresponds to the 6th root of the MRCI matrix, while the $^3A''$ one to its 5th root. This is due to the fact that there are six lower lying molecular states resulting from the interaction of He with I_2 states of triplet spin character originating from the ground state atomic I fragments, i.e., $^3(\Sigma_u^{+\,2}, \Sigma_g^-, \Pi_g, \Pi_g, \Delta_u)$, that under C_s symmetry split into five $^3A'$ and four $^3A''$ states. Size non-extensivity errors were accounted for by the multireference analog of the Davidson correction, denoted as +Q in what follows.[36] The active space of our zeroth order wavefunction contains, in addition to the plain valence shell, four orbitals of Rydberg character. The resulting MRCI space contains 23.7× 10^9 configuration functions (CF) internally contracted to ≈ 136 × 10^6 CF under C_s symmetry restrictions. Size non-extensivity errors amount to 35(2) mE_h at the MRCI(+Q) level of theory.

In the presence of SO coupling, the two $^3A'$ and $^3A''$ states of He–I_2(E) are mixed. The SO splitting of the three I_2(E$^3\Pi_g$) states, namely, $^3\Pi_{0_g^+}$, $^3\Pi_{1_g}$, and $^3\Pi_{2_g}$, is 3–4 orders of magnitude larger than the minute difference of the $^3A'$ and $^3A''$ states. Thus, when these states are interacting with a He atom the SO coupling effect can be approximated by the semi-sum of the adiabatic $^3A'$ and $^3A''$ potentials, their difference being negligible. Although no explicit SO calcu-

lations have been performed here for He–I_2(E), one can see based on MRCI and MRCI+SO results of the diatomic I_2 and He–I_2(B) molecules,[26,28] as well as on previous studies of similar triatomic complexes,[23,37–41] that this is indeed an excellent approximation. Therefore, the interaction potential for the $E^3\Pi_{0_g^+}$ state approximately modified by spin–orbit coupling is given by the average of the $^3A'$ and $^3A''$ potentials, $V_E = \frac{V_{^3A'}+V_{^3A''}}{2}$.

B. Representation of the potential energy surface

For the representation of the PES, we used an interpolation process within the reproducing kernel space (RKHS) method by Ho and Rabitz.[42] It consists in expressing the interaction energy as

$$V_E(R,\theta;r_e) = \sum_{i=1}^{N_R}\sum_{j=1}^{N_\theta} v_{ij} q_1^{2,5}(R_i, R) q_2(y_j, y), \quad (1)$$

where $y = \cos\theta$, N_R and N_θ is the number of the calculated *ab initio* points in R and θ coordinates, respectively. The $q_1^{n,m}$ and q_2 are the one-dimensional reproducing kernel functions for the distance-like, R, and angle-like, θ, variables, respectively, given[42] by

$$q_1^{n,m}(x,x') = n^2 x_>^{-(m+1)} B(m+1,n) \times {}_2F_1\left(-n+1, m+1; n+m+1; \frac{x_<}{x_>}\right), \quad (2)$$

$$q_2(y,y') = \sum_l \frac{(2l+1)}{2} P_l(y) P_l(y') \quad (3)$$

with, $x_>$ and $x_<$ are the largest and smallest value of the x and x', respectively. The superscripts n and m refer to the order of smoothness of the function, and its asymptotic behavior at large distances, B is the beta function, ${}_2F_1$ is the Gauss hyper-geometric function. The P_l are the Legendre polynomials with $l = 0$, 2, 4, 6, 8, 10, 12, 14, 16, and 18 in the present case. The linear coefficients, v_{ij}, are obtained as solutions of Eq. (1), where $V(R_i, \theta_j; r_e)$ is the average value of the calculated MRCI+Q interaction energies of $^3A'$ and $^3A''$ symmetry at the $(R_i, \theta_j; r_e)$ grid point, with $i = 1$–N_R and $j = 1$–N_θ.

C. Bound state calculations

As it has been already stated the $^3A'$ and $^3A''$ states are coupled via the SO coupling operator, and an effective Hamiltonian including the SO term should have been employed (see Refs. 37–39) for dynamics calculations. However, in the atom-diatom case, and following the formalism described in Refs. 37 and 38 for a diatom in the $^3\Pi_0$ state, the matrix elements of the interaction potential can be represented by the semi-sum of the adiabatic potentials, and a spin-free closed-shell-type rovibrational Hamiltonian is employed here, as in previous studies of such systems,[13,23,26,40] to study the nuclear dynamics. The two-dimensional operator in the Jacobi coordinate system reads

$$\hat{H} = -\frac{\hbar^2}{2\mu_1}\frac{\partial^2}{\partial R^2} + \frac{\hat{l}^2}{2\mu_1 R^2} + \frac{\hat{j}^2}{2\mu_2 r_e^2} + V_E(R,\theta;r_e), \quad (4)$$

where, $\hat{l}$ and $\hat{j}$ are the angular momentum operators associated with the vectors **R** and **r**, respectively, leading to a total angular momentum $\hat{J} = \hat{l} + \hat{j}$, $\frac{1}{\mu_1} = \frac{1}{m_{He}} + \frac{1}{2m_I}$, $\frac{1}{\mu_2} = \frac{1}{m_I} + \frac{1}{m_I}$, $m_{He} = 4.00260$ amu, $m_I = 126.904473$ amu, and $V_E(R, \theta; r_e)$ is given by Eq. (1). The r(I–I) interatomic distance is fixed at the equilibrium value of $r_e = 3.5931$ Å. The bound vdW levels and corresponding wavefunctions are calculated variationally by diagonalizing the two-dimensional Hamiltonian matrix.

As previously done in similar vdW systems,[22,43,44] the corresponding Hamiltonian (see Eq. (4)) is represented in a space composed of products of radial and angular basis functions. For the R coordinate, a basis set of 160 discrete variable representation functions over the range $3 \le R \le 15$ Å, is used based on the particle in a box eigenfunctions,[45] while for the θ coordinate the orthonormalized Legendre polynomials $P_j(\cos\theta)$ with j values ranging from 0 to 79, for the diatomic rotation are employed. In this way, a convergence of 0.001 cm^{-1} is achieved in bound state calculations for the ten lowest vdW vibrational ($J = 0$) levels of He–I_2(E).

III. RESULTS AND DISCUSSION

In Table I, we list total energies, equilibrium distances, well-depths with respect to the corresponding dissociation channels and adiabatic excitation energies for the ground X, valence B and ion-pair E states. At the MRCI+Q level of theory, the E state is located at 44482 cm^{-1} above the global potential minimum of the ground X state (as calculated at the CCSD(T) level). By comparing the T_e^E of HeI_2 with the one of I_2 at 41457 cm^{-1},[28] we obtain a difference of 3025 cm^{-1} due to the different (CCSD(T) and MRCI+Q) methods employed here for the X and E states. Also from CCSD(T) calculations we estimated the excitation energy of the B state, $T_e^B = 12534$ cm^{-1}. These values do not include the SO

TABLE I. Total energies E_e (in a.u.), equilibrium distances R_e (in Å), dissociation energies D_e (in cm^{-1}), and energy gaps T_e (in cm^{-1}) for the indicated electronic states of the HeI_2 vdW complex. These values are obtained by CCSD(T), for the ground X and excited valence B states, and MRCI+Q, for the E state, calculations using the ECP28MDF/AV5Z-PP/AVQZ basis sets. For the B and E states we used the averaged value of the $^3A'$ and $^3A''$ states. Comparison with previous calculations (in parenthesis) is also presented.

	X state		Bstate	Estate
Config.	Linear	T-shaped	T-shaped	T-shaped
E_e	−592.61674	−596.61670	−592.55963	−592.41406
R_e	4.88 (4.83[a])	3.83 (3.82[a])	3.97 (3.96[b])	4.13
D_e	45.21 (44.28[a])	37.75 (38.92[a])	29.63 (29.48[b])	33.14
T_e	0	...	12534	44482

[a]From RCCSD(T)/ECP28MDF/AV(Q/5)Z-PP/AV(Q/5)Z calculations extrapolated at the CBS[Q5] limit, see Ref. 22.
[b]From UCCSD(T)/ECP28MDF/AV5Z-PP/AV(Q/5)Z calculations, see Ref. 26.

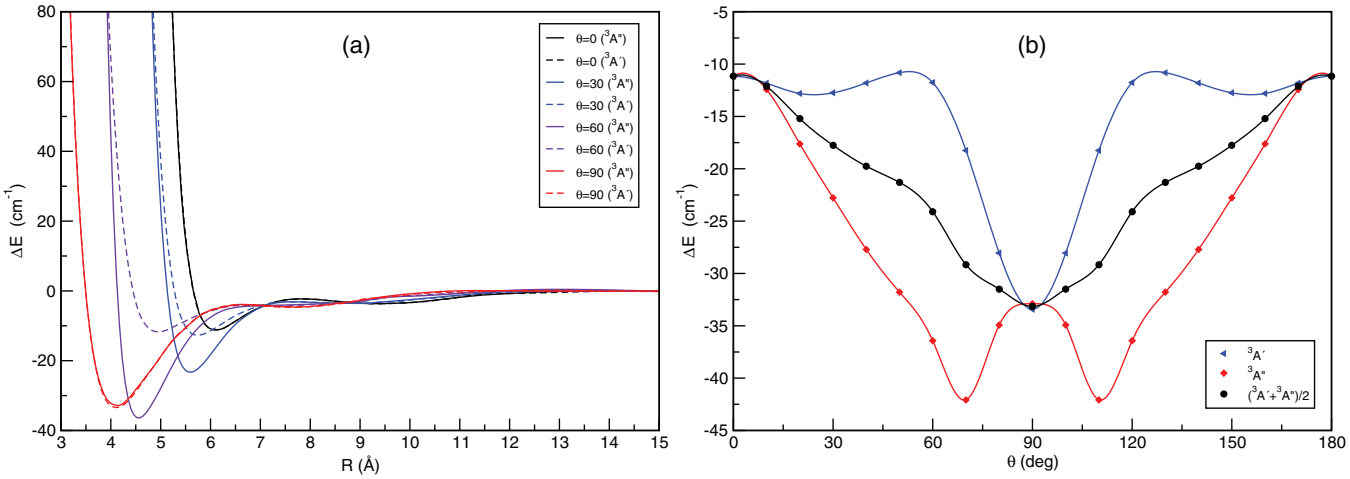

FIG. 1. MRCI+Q interaction energies of the $^3A'$ (dashed lines) and $^3A''$ (solid lines) states as a function of R at the indicated θ angles (left panel), and MRCI+Q minimum energy path of $^3A'$, $^3A''$ and their averaged values as a function of θ (right panel).

effects, of about 3065 cm^{-1} from previous MRCI+SO calculations of the B state.[26]

Figure 1 shows the interaction potentials of $^3A'$ and $^3A''$ symmetries at the MRCI+Q level of theory, as a function of R for four selected θ values, $\theta = 0^\circ$ ($C_{\infty v}$), 30°, 60°, and $\theta = 90^\circ$ (C_{2v}) (see left panel). In the right panel of Fig. 1, we display the minimum energy path for both $^3A'$ and $^3A''$ potentials as a function of θ by optimizing at each angle the R coordinate.

In Figure 2, we present a valence bond diagram of the ion-pair E $I_2(^3\Pi_g)$ state interacting with the He atom at C_s symmetry. As the He atom approaches the I_2 molecule, the system lowers its symmetry from $D_{\infty h}$ to C_s, and consequently the electronic wavefunction does not display the g symmetry anymore but at $\theta = 90^\circ$ (C_{2v}) the two I atoms are identical. At linear configurations the two states are degenerate. When $\theta \neq 90^\circ$ a charge asymmetry shows up between the two I atoms with the positive end located on the I atom that is closer to He. This leads to a more attractive interaction when the symmetry defining electron is perpendicular to the molecular plane, i.e., at $^3A''$ symmetry and $\theta \sim 70^\circ$ (see Fig. 1). As we move on at smaller angle values the interaction energy drops to $\sim$10 cm^{-1}. In all cases, the interaction energy for the $^3A''$ symmetry is larger than that for the $^3A'$ one, since the symmetry defining electron is off the way of the He atom

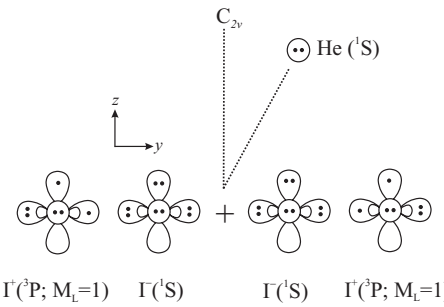

FIG. 2. Schematic valence bond description of the He…$I_2(E^3\Pi_g)$ system.

(see Fig. 1). In general, the two states show distinct topologies. For example, the $^3A'$ has a minimum for the T-shaped configuration with a well-depth of 33.4 cm^{-1}, and two shallow ones around 25° and 155°, respectively, at an energy of -12.9 cm^{-1}, while the $^3A''$ one has a symmetric double minimum at 70° and 110° with well-depths of 42.0 cm^{-1}, while the T-shaped structure at -32.9 cm^{-1} corresponds to a saddle point connecting them. A common feature of both states is the presence of a local minimum at all angles and at large R distances (see Fig. 1, right panel). The computed MRCI and MRCI+Q interaction energies for the $^3A'$ and $^3A''$ states of the $HeI_2(E)$ for each θ and R values are listed in the supplementary material.[46] In Fig. 1 (see right panel), we also plot the minimum energy path of their averaged value, $\frac{^3A'+^3A''}{2}$. One can see that the T-shaped configuration is the global minimum with $D_e = 33.2$ cm^{-1}, while the linear one at energy of -11.2 cm^{-1} is a saddle point. Further, we should mention a rather wide plateau for angles between 25° and 60° that reflects the region of major differences between the two states.

Given the complicated topology, with the presence of multiple minima along the R coordinate, the representation of the PES using an analytical form, such as in the previous studies of similar vdW clusters, is not a straightforward task. Therefore, we consider that a more efficient way for constructing a smooth potential surface from the *ab initio* data could be to employ the general interpolation method based on the RKHS and the inverse problem theory,[42] as described above (see Sec. II B).

In Figure 3, we present a three-dimensional plot of the RKHS PES, Eq. (1), V(R, θ; $r_e = 3.5931$ Å) in the (θ, R) plane, while in Figs. 4 and 5 we display the minimum energy path along the θ coordinate, and the potential curves at the indicated θ values as a function of the distance R, respectively. In Table II, we list the main characteristics of the present surface, and we compare them with the ones available from the DIM-PT1 (diatomics-in-molecule first-order perturbation theory) approach.[32] The MRCI+Q/RKHS PES predicts the global minimum at an energy of -33.18 cm^{-1} with $R = 4.10$ Å and $\theta = 90^\circ$. One can see that both MRCI+Q

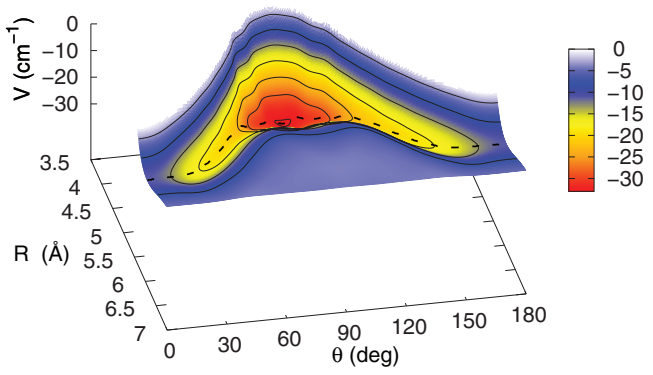

FIG. 3. Three-dimensional plot of the $V(R,\theta)$ (in cm^{-1}) potential energy surface of Eq. (1) of the E HeI_2 state. The I_2(E) is fixed at its equilibrium distance $r_e = 3.5931$ Å. The minimum energy path (dashed line) is also shown.

and DIM-PT1 surfaces predict the global minimum at a T-shaped configuration, with the linear geometry corresponding to a saddle point. However, the DIM-PT1 PES clearly overestimates the well-depth of the global minimum by ∼20 cm^{-1}, while the energy of the linear saddle point differences by only 3 cm^{-1}.

The major new feature of the MRCI+Q PES (see Fig. 4), as compared to the previous *ab initio* PESs of the X and B HeI_2 states,[21,22,26] is the existence of local minima at 7.7 Å ($\theta = 90^\circ$) and at 9.3 Å ($\theta = 0^\circ$) at −4.6 cm^{-1} and −3.7 cm^{-1}, respectively. The barrier between the global and local minima are at $R = 6.6$ Å and energy of −3.9 cm^{-1}, and $R = 7.8$ Å and energy of −2.3 cm^{-1} for the T-shaped and linear configurations, respectively. We should mention that this shallow minimum at large R values, between 8.0 and 9.5 Å with energies ranging from −5.5 to −3.5 cm^{-1}, is present at all θ values for both $^3A'$ and $^3A''$ symmetries (see Fig. 1). Its existence should be due to the electronic ion-pair character of the I_2 E state since it is absent in both the X and B PES of the He–I_2 vdW complex. As it can be seen in Figs. 3 and 4, the surface presents a plateau for angles between 30° and 60°, showing a larger anisotropy around the T-shaped well as compared to

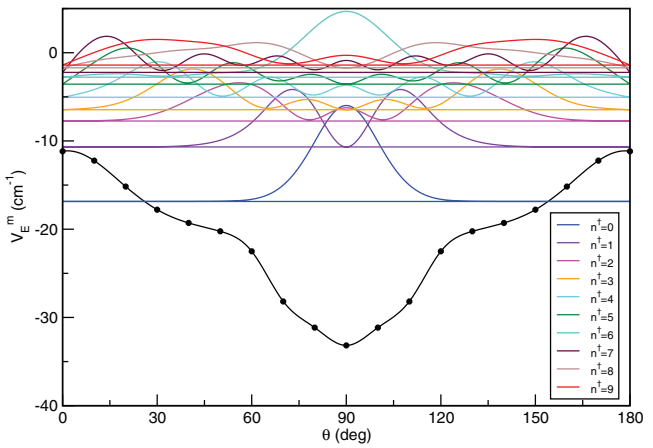

FIG. 4. Minimum energy path, V_E^m, of the E HeI_2 state as a function of θ obtained from the RKHS interpolation (see Eq. (1)). The energies and angular probability distributions of the lowest ten bound intermolecular vdW levels for $J = 0$ are also displayed. The zero probability for each eigenstate is shifted to its eigenenergy (see Table IV).

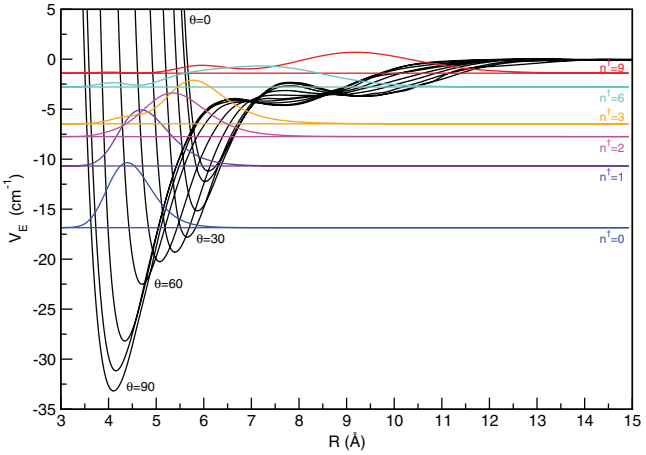

FIG. 5. The interaction potential curves as a function of R of the HeI_2 obtained from the RKHS interpolation (see Eq. (1)). The energies and radial probability distributions of the indicated $n^\dagger$ bound intermolecular vdW levels for $J = 0$ are also displayed. The zero probability for each eigenstate is shifted to its eigenenergy (see Table IV).

the PESs of the X and B states of this complex.[21,22,26] The accuracy of the RKHS interpolation is checked by comparing with additional MRCI+Q *ab initio* points not included in the interpolation scheme. In Table III, we list for some selected configurations of them along the minimum energy path, the RKHS potential value, together with the MRCI+Q interaction energy and the difference between them. In total, we obtained an averaged deviation of 0.1 cm^{-1} for the RKHS PES with respect to the MRCI+Q energies.

Using the RKHS PES, we performed nuclear bound state calculations, as described in Sec. II C. The energies of the ten lowest vibrational levels of He–I_2(E) vdW complex are listed in Table IV, while their corresponding angular and radial distributions are displayed in Figs. 4 and 5, respectively. Our calculations predict these states at energies of −16.85 (even), −10.68 (odd), −7.74 (even), −6.46 (odd), −5.05 (even), −3.56 (odd), −2.78 (even), −2.23 (even), −1.71 (odd), and −1.40 (even) cm^{-1}, with even/odd symmetry with respect to the diatomic $j^\dagger$ rotation. As can be seen in Fig. 4 the $n^\dagger = 0$ is strictly localized at a $\theta = 90^\circ$ configuration, while the $n^\dagger = 6$ vdW level presents its maximum probability also at C_{2v} structure with some delocalization at near linear geometries. The first excited vibrational level is localized around $\theta = 70^\circ$ and 110°, while the $n^\dagger = 2$, 3, 4, and 5 vibrational levels present an "interesting" oscillating pattern, spreading over the whole range of θ, and with their corresponding probability maxima located at ∼55°, 40°, 30°, and 20° θ values, respectively, while their secondary maxima converge towards T-shaped nuclear arrangements. The two most excited vibrational levels, $n^\dagger = 8$ and 9, present a highly fluxional behavior rendering a floppy character to the corresponding states. The radial distributions provide also interesting comments (see Fig. 5). The ground vdW level is located at $R_0 = 4.4$ Å, while the corresponding values of the $n^\dagger = 1$–5 levels increase monotonically up to ∼6 Å ($n^\dagger = 5$). As we move on to higher energies the radial distributions acquire double maxima at both small and large R values due to the double minima character of the underlying PES.

TABLE II. Well-depths, and equilibrium distances for the He–I_2(E) complex at the indicated orientations. Its binding energy, D_0, is also given.

	$\theta = 90^\circ$ Global (Local) minimum			$\theta = 0^\circ$ Saddle points	
He–I_2(E)	D_e	D_0	R_e	D_e[a]	R_e[a]
This work	33.178 (4.62)	16.85	4.10 (7.67)	11.17 (3.69)	6.11 (9.32)
DIM-PT1 value[32]	52.7	...	3.62/–	14.3	6.39
Experimental value[13]	...	16.7±0.6	...	...	...

[a]Linear saddle points energies and geometries.

This is more pronounced for the $n^\dagger = 8$ and $n^\dagger = 9$ levels. The $n^\dagger = 6$ level has also a highly irregular R distribution, since it is mostly located in the shallow well at large R for $\theta = 90^\circ$, as we can see from its angular distribution.

The only available experimental results on the He–I_2 E state was published by the Loomis group[13] and are limited to the binding energies of the three lowest levels $n^\dagger = 0$, 1, and 2 of the He–I_2(E, $v^\dagger = 1$) at 16.7 ± 0.6, 14.1 ± 0.6, and 10.7 ± 0.6 cm^{-1}, respectively (see Table IV). Moreover, the experiment predicts a T-shaped isomer for the E state of the HeI_2, and as we can see its calculated structure and binding energy are in excellent accord with the experimental measurements. However, for the next two, $n^\dagger = 1$ and 2, vibrational levels we find (see Table IV) differences of 3.4 and 3.0 cm^{-1}, respectively, compared with the ones obtained from the RKHS PES. At a first glance, these deviations can be attributed to the errors in the *ab initio* calculations, approximations for including the spin-orbit effects, and thus in the construction of the PES, which was not able to reproduce correctly the anharmonicity of the potential well. We can also see that the $n^\dagger = 1$ level is predicted by the RKHS PES to be at almost the same energy, just a difference of 0.02 cm^{-1}, with the $n^\dagger = 2$ level of the experimental observations. Thus, we should further analyze the experimental conditions and the corresponding assignment in order to gain some insights into the underlying dynamics and possible reasoning for the disagreement obtained with the data of the present intermolecular PES. The recorded two-color, pump-probe spectra show three features (see Fig. 4 in Ref. 13) at total excitation energies of around 41456, 41458.5, and 41463.5 cm^{-1}, respectively. The pump laser was fixed in the $n' = 0$, and 3 features of the I_2 B–X, 23–0 region, the probe laser scanned the I_2 E–B, 1–23 region, and these peaks have been assigned[13] to transitions from the $n' = 0$ or 3 levels of the He–I_2(B, $v' = 23$) → He–I_2(E, $v^\dagger = 1$) with $n^\dagger = 0$, 1, and 2 (see Table IV). In Figure 6, we show the angular distributions and energies of the involved vibrational levels for each electronic state as they are predicted in the present and previous theoretical studies,[22,26] together with the experimentally assigned transitions.

TABLE III. The MRCI+Q ($\frac{^3A'+^3A''}{2}$) interaction energies in comparison with the RKHS potential values at the indicated (θ, R) points along the minimum energy path of the E HeI_2 state.

(θ, R)	E(MRCI+Q)	$V_E(R, \theta; r_e)$	E(MRCI+Q)-V_E
(0,6.0974)	−11.26	−11.17	−0.082
(4,6.0874)	−11.37	−11.34	−0.115
(8,6.0473)	−11.78	−11.84	0.062
(10,6.0272)	−12.20	−12.23	0.031
(14,5.9771)	−13.34	−13.26	−0.083
(18,5.9069)	−14.63	−14.51	−0.122
(20,5.8668)	−15.24	−15.17	−0.078
(26,5.7464)	−16.99	−16.95	−0.040
(30,5.6562)	−17.88	−17.79	−0.088
(34,5.5458)	−18.68	−18.51	−0.170
(40,5.3954)	−19.36	−19.30	−0.062
(45,5.2249)	−19.88	−19.90	0.025
(50,5.0745)	−20.36	−20.25	−0.113
(52,4.9842)	−20.64	−20.56	−0.079
(60,4.7034)	−22.53	−22.51	−0.019
(62,4.6132)	−23.40	−23.25	−0.155
(67,4.4327)	−26.43	−26.57	0.137
(70,4.3424)	−28.28	−28.19	−0.093
(75,4.2321)	−30.49	−30.16	0.330
(80,4.1519)	−31.29	−31.17	−0.124
(90,4.1017)	−33.16	−33.18	0.014

Based on theoretical calculations of the vibrational levels for each electronic state, and taking into account the Franck-Condon factors, one can see that the transition from the $n' = 0$ → $n^\dagger = 0$ corresponds to the highest relative intensity feature, in agreement with the experiment. It turns out, that a possible proposed scenario, based on the available theoretical information for the next two observed features, could attribute them to transitions from the $n' = 1 \rightarrow n^\dagger = 1$ and $n' = 0 \rightarrow n^\dagger = 1$ states, which are shifted in energy by 2.09 and 6.17 cm^{-1}, respectively. These values are in excellent accord (see Table IV) with the experimental reported energy shifts;[13] however, we should stress that in the experimental setup only the $n' = 0$ or 3 states are involved, and thus the theoretical assignment of the second peak is rather questionable. Further, we should mention that the $n' = 1$ state was the only vibrational level of the B state that has not been detected from the experiment, while all the other vibrational states have been obtained,[13] and this might be an argument for further investigation. Also, as we pointed out above, in the experimental setup the X, B, and E states of the HeI_2 are involved, and one can see that for the X state the linear and T-shaped $n'' = 0$, 1, and 2 states are very close in energy (see Fig. 6), with a difference of 0.3 (in reverse ordering) and 0.2 cm^{-1} based on the experimental and theoretical predictions,[13,22] respectively. In any case, we should say that the present theoretical estimates are for zero temperature, while experimental measurements have been recorded

TABLE IV. Theoretical and experimental energies (in cm^{-1}) for the bound vibrational vdW levels of HeI_2(E), together with theoretical and experimental values for the energy shifts of the indicated E ← B transitions.

			This work/Expt.	
$n^\dagger$	This work (2D) RKHS PES	Expt. [13] He + I_2(E, $v^\dagger = 1$)	(E,$r = r_e$) ← (B,$v' = 20$)/(E,$v^\dagger = 1$) ← (B,$v' = 23$) ($n^\dagger$, $J^{p\dagger}$, $j^\dagger$) ← (n', $J^{p'}$, j')/$n^\dagger$ ← n'	Energy shift
0	− 16.85	-16.7 ± 0.6	$(0,0^+,e) \leftarrow (0,1^-,o)/0 \leftarrow 0$ or 3	0.0/0.0
1	− 10.68	-14.1 ± 0.6	$(1,0^+,o) \leftarrow (1,1^-,e)/1 \leftarrow 0$ or 3	$2.09/2.6 \pm 0.6$
2	− 7.74	-10.7 ± 0.6	$(1,0^+,o) \leftarrow (0,1^-,e)/2 \leftarrow 0$ or 3	$6.17/6 \pm 0.6$
3	− 6.46	…	…	…
4	− 5.05	…	…	…
5	− 3.56	…	…	…
6	− 2.78	…	…	…
7	− 2.23	…	…	…
8	− 1.71	…	…	…
9	− 1.40	…	…	…

at a low temperature regime (T ≤ 1 K), where rovibrational states with $J'' < 9$ were significantly populated,[13] and does not facilitate detailed comparisons.

Unfortunately, no more experimental and/or theoretical data are up to now available in order to justify our assertion, and thus to further evaluate the present surface.

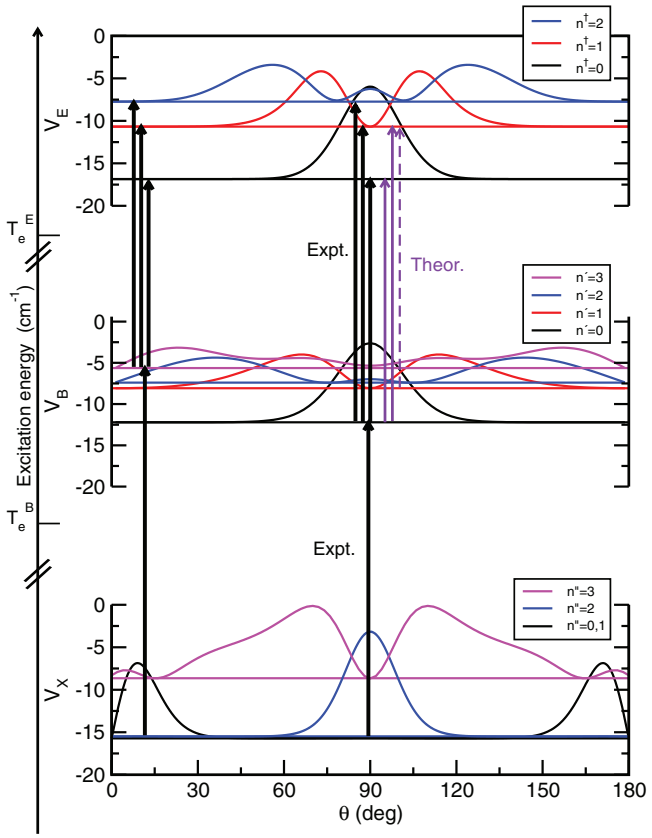

FIG. 6. Vibrational energies and corresponding angular distributions for the three electronic states, ground X, valence B, and ion-pair E, as calculated in the present and previous theoretical studies[22,26] being involved in the experimental spectra[13] of the HeI_2 molecule. The inter y axes correspond to the interaction potential energies for each state, while the outer y axis indicates the total excitation energy. T_e^B and T_e^E indicate the adiabatic excitation energies for the B and E states, respectively, (see Table I). Transitions corresponding to the experimental and theoretical assignments are also shown (see Table IV).

IV. CONCLUSIONS

We present for the first time high level *ab initio* results on the electronic excited E state of the HeI_2 vdW system based on large MRCI+Q calculations in conjunction with ECP and large basis sets. Interaction energies were calculated at a frozen $r = r_e$ distance for the I_2 moiety for a grid of several points in the R and θ coordinates for values between 3.0 and 30.0 Å and 0° and 90°, respectively, for the $^3A'$ and $^3A''$ states which correlate with the $^3\Pi_g$ ion-pair state of I_2. The surface is approximated by the semi-sum of the spin-free $^3A'$ and $^3A''$ interaction potentials. Given the complicated morphology of this ion-pair character PES, an interpolation scheme based on the RKHS method has been adopted for its representation. The surface presents a global minimum for the T-shaped configuration with a well-depth of 33.18 cm^{-1}, a local one at energy of -4.62 cm^{-1}, saddle points for linear structures and a wide plateau for intermediate bending geometries.

Variational bound state calculations were performed for the RKHS PES and the lowest ten bound vibrational states of the HeI_2(E) cluster were determined. The binding energy, D_0, is calculated to be 16.85 cm^{-1}, with the corresponding wavefunction being located at the T-shaped structure. These findings are in excellent agreement with the available experimental data on the $n^\dagger = 0$ level of the He..I_2(E, $v^\dagger = 1$) from a two-color, pump-probe spectra recorder in the I_2 B–X, 23–0, and E–B, 1–23 regions. The next two vibrational levels are calculated at energies of -10.68 and -7.74 cm^{-1}, while the experimental ones have been set to -14.1 ± 0.6 and -10.7 ± 0.6, respectively. Higher vibrational states are also obtained, and we found that their probability distributions clearly reflect the large anisotropy of the underlying PES. Based on the theoretical predictions for all three (X, B, and E) involved electronic states of HeI_2, we discussed different possible scenaria in order to analyze our results in comparison with the experimental assignments for these energy levels aiming in this way to understand the source of the disagreement. We may conclude that both experimental conditions and theoretical treatments do not facilitate a detailed comparison, so additional observations and calculations are in order.

The study of electronically excited vdW systems presents a challenge for the theory of intermolecular interactions, and here we demonstrate to what extent *ab initio* computations can reach. We found that highly electronic excited interaction energies for such vdW systems can be determined, providing a reliable and accurate description for the E state PES of the HeI_2, that in combination with the ground X and electronic excited B state of the complex, is useful to model experimental data related to potential minima and also predict higher vibrational vdW states. However, for a further evaluation of the surface it is clear that more experimental data are required, together with the corresponding theoretical simulations.

ACKNOWLEDGMENTS

The authors thank to Centro de Calculo (IFF), CTI (CSIC), and CESGA for allocation of computer time. This work has been supported by the MICINN Grant Nos. FIS2010-18132 and FIS2011-29596-C02-01.

[1]See the thematic issues on van der Waals molecules, Chem. Rev. **88** (1988), **94** (1994), **100** (2000).
[2]D. H. Levy, Adv. Chem. Phys. **47**, 323 (1981).
[3]M. Gutmann, D. M. Willberg, and A. H. Zewail, J. Chem. Phys. **97**, 8048 (1992).
[4]A. Rohrbacher, N. Halberstadt, and K. C. Janda, Ann. Rev. Phys. Chem. **51**, 405 (2000).
[5]J. M. Pio, M. A. Taylor, W. E. van der Veer, C. R. Beiler, J. A. Cabrera, and K. C. Janda, J. Chem. Phys. **133**, 014305 (2010).
[6]D. S. Boucher and R. A. Loomis, Adv. Chem. Phys. **138**, 375 (2008).
[7]A. A. Buchachenko, R. Prosmiti, C. Cuhna, P. Villarreal, and G. Delgado-Barrio, J. Chem. Phys. **117**, 6117 (2002).
[8]C. Diez-Pardos, Á. Valdés, R. Prosmiti, P. Villarreal, and G. Delgado-Barrio, Theor. Chem. Acc. **118**, 511 (2007).
[9]R. E. Smalley, D. H. Levy, and L. Wharton, J. Chem. Phys. **64**, 3266 (1976).
[10]R. E. Smalley, L. Wharton, and D. H. Levy, J. Chem. Phys. **68**, 671 (1978).
[11]J. A. Blazy, B. M. DeKoven, T. D. Russell, and D. H. Levy, J. Chem. Phys. **72**, 2439 (1980).
[12]D. G. Jahn, S. G. Clement, and K. C. Janda, J. Chem. Phys. **101**, 283 (1994).
[13]S. E. Ray, A. B. McCoy, J. J. Glennon, J. P. Darr, E. J. Fesser, J. R. Lancaster, and R. A. Loomis, J. Chem. Phys. **125**, 164314 (2006).
[14]A. E. S. Miller, C.-C. Chuang, H. C. Fu, K. J. Higgins, and W. Klemperer, J. Chem. Phys. **111**, 7844 (1999).
[15]A. Burroughs and M. C. Heaven, J. Chem. Phys. **114**, 7027 (2001).
[16]A. Burroughs, G. Kerenskaya, and M. C. Heaven, J. Chem. Phys. **115**, 784 (2001).
[17]R. Prosmiti, C. Cunha, P. Villarreal, and G. Delgado-Barrio, J. Chem. Phys. **117**, 7017 (2002).
[18]R. Prosmiti, P. Villarreal, and G. Delgado-Barrio, Chem. Phys. Lett. **359**, 473 (2002).
[19]Á. Valdés, R. Prosmiti, P. Villarreal, and G. Delgado-Barrio, Chem. Phys. Lett. **375**, 328 (2003).
[20]Á. Valdés, R. Prosmiti, P. Villarreal, and G. Delgado-Barrio, Mol. Phys. **102**, 2277 (2004).
[21]R. Prosmiti, Á. Valdés, P. Villareal, and G. Delgado–Barrio, J. Phys. Chem. A **108**, 6065 (2004).
[22]L. García-Gutierrez, L. Delgado-Tellez, Á. Valdés, R. Prosmiti, P. Villarreal, and G. Delgado-Barrio, J. Phys. Chem. A **113**, 5754 (2009).
[23]J. Williams, A. Rohrbacher, J. Seong, N. Marianayagam, K. C. Janda, R. Burcl, M. M. Szcześniak, G. Chalasiński, S. M. Cybulski, and N. Halberstadt, J. Chem. Phys. **111**, 997 (1999).
[24]M. P. de Lara-Castells, A. A. Buchachenko, G. Delgado-Barrio, and P. Villarreal, J. Chem. Phys. **120**, 2182 (2004).
[25]R. Hernández-Lamoneda and K. C. Janda, J. Chem. Phys. **123**, 161102 (2005).
[26]Á. Valdés, R. Prosmiti, P. Villarreal, G. Delgado-Barrio, and H.–J. Werner, J. Chem. Phys. **126**, 204301 (2007).
[27]R. S. Mulliken, J. Chem. Phys. **55**, 288 (1971).
[28]A. Kalemos, Á. Valdés, and R. Prosmiti, J. Phys. Chem. A **116**, 2366 (2012).
[29]T. V. Tscherbul, A. A. Buchachenko, M. E. Akopyan, S. A. Poretsky, A. M. Pravilov, and T. A. Stephenson, Phys. Chem. Chem. Phys. **6**, 3201 (2004).
[30]M. E. Akopyan, I. Yu. Novikova, S. A. Poretsky, A. M. Pravilov, A. G. Smolin, T. V. Tscherbul, and A. A. Buchachenko, J. Chem. Phys. **122**, 204318 (2005).
[31]C. J. Fecko, M. A. Freedman, and T. A. Stephenson, J. Chem. Phys. **116**, 1361 (2002).
[32]T. V. Tscherbul, Yu. V. Suleimanov, and A. A. Buchachenko, Russ. J. Phys. Chem. **80**, 1957 (2006).
[33]K. A. Peterson, B. C. Shepler, D. Figgen, and H. Stoll, J. Phys. Chem. A **110**, 13877 (2006).
[34]D. E. Woon and T. H. Dunning,Jr., J. Chem. Phys. **100**, 2975 (1994).
[35]H.-J. Werner, P. J. Knowles, F. R. Manby, M. Schütz *et al.*, MOLPRO, version 2006.1, a package of *ab initio* programs, 2006, see http://www.molpro.net.
[36]S. R. Langhoff and E. R. Davidson, Int. J. Quantum Chem. **8**, 61 (1974); E. R. Davidson and D. W. Silver, Chem. Phys. Lett. **52**, 403 (1977).
[37]M. H. Alexander and B. Pouilly, J. Chem. Phys. **79**, 1545 (1983).
[38]M. H. Alexander, Chem. Phys. **92**, 337 (1985).
[39]M.-L. Dubernet, D. Flower, and J. M. Hutson, J. Chem. Phys. **94**, 7602 (1991).
[40]D. S. Boucher, D. B. Strasfeld, R. A. Loomis, J. M. Herbert, S. A. Ray, and A. B. McCoy, J. Chem. Phys. **123**, 104312 (2005).
[41]R. J. Doyle, D. M. Hirst, and J. M. Hutson, J. Chem. Phys. **125**, 184312 (2006).
[42]T-S. Ho and H. Rabitz, J. Chem. Phys. **104**, 2584 (1996).
[43]R. Prosmiti, C. Cunha, P. Villarreal, and G. Delgado-Barrio, J. Chem. Phys. **119**, 4216 (2003).
[44]L. Delgado-Tellez, A. Valdés, R. Prosmiti, P. Villarreal, and G. Delgado-Barrio, J. Chem. Phys. **134**, 214304 (2011).
[45]J. T. Muckerman, Chem. Phys. Lett. **173**, 200 (1990).
[46]See supplementary material at http://dx.doi.org/10.1063/1.4733983 for the computed interaction energies.